1521-009X/43/12/1905–1916$25.00
Drug Metabolism and Disposition

http://dx.doi.org/10.1124/dmd.115.065763
Drug Metab Dispos 43:1905–1916, December 2015

In Vitro Metabolism of Montelukast by Cytochrome P450s and UDP-Glucuronosyltransferases

Josiane de Oliveira Cardoso, Regina Vincenzi Oliveira, Jessica Bo Li Lu, and Zeruesenay Desta

Department of Medicine, Division of Clinical Pharmacology, Indiana University School of Medicine, Indianapolis, Indiana (J.O.C.; J.B.L.L. and Z.D.); Department of Chemistry, Federal University of São Carlos, São Carlos, SP, Brazil (J.O.C. and R.V.O.)

Received May 31, 2015; accepted September 14, 2015

ABSTRACT

Montelukast has been recommended as a selective in vitro and in vivo probe of cytochrome P450 (P450) CYP2C8 activity, but its selectivity toward this enzyme remains unclear. We performed detailed characterization of montelukast metabolism in vitro using human liver microsomes (HLMs), expressed P450s, and uridine 5′-diphospho-glucuronosyltransferases (UGTs). Kinetic and inhibition experiments performed at therapeutically relevant concentrations reveal that CYP2C8 and CYP2C9 are the principal enzymes responsible for montelukast 36-hydroxylation to 1,2-diol. CYP3A4 was the main catalyst of montelukast sulfoxidation and stereoselective 21-hydroxylation, and multiple P450s participated in montelukast 25-hydroxylation. We confirmed direct glucuronidation of montelukast to an acyl-glucuronide. We also identified a novel peak that appears consistent with an ether-glucuronide. Kinetic analysis in HLMs and experiments in expressed UGTs indicate that both metabolites were exclusively formed by UGT1A3. Comparison of in vitro intrinsic clearance in HLMs suggest that direct glucuronidation may play a greater role in the overall metabolism of montelukast than does P450-mediated oxidation, but the in vivo contribution of UGT1A3 needs further testing. In conclusion, our in vitro findings provide new insight toward montelukast metabolism. The utility of montelukast as a probe of CYP2C8 activity may be compromised owing to involvement of multiple P450s and UGT1A3 in its metabolism.

Introduction

Montelukast (Fig. 1), (*R*)-1-[(1-(3-(2-(7-chloro-2-quinolinyl)-ethenyl) phenyl)-3-(2-(2-hydroxy-2-propyl)phenyl)propyl)thiomethyl] cyclopropane acetic acid, is a potent and selective antagonist of the cysteinyl leukotriene receptor 1 subtype (CysLT1) (De Lepeleire et al., 1997; Jones et al., 2001). Thus, it effectively reverses adverse consequences of leukotriene D4 (LTD4)-mediated $CysLT_1$-receptor activation on the airway of the lung (Dahlen et al., 1980; Lewis et al., 1990) and is widely used for the prophylaxis and treatment of asthma and seasonal allergies in children and adults (Reiss et al., 1996; Knorr et al., 1998).

Studies in health volunteers administered [^{14}C]montelukast indicate that approximately 86% of the administered dose is recovered in feces and only ≤0.2% recovered in urine (Balani et al., 1997). It is believed that ~58% of the orally administered dose is absorbed to the systemic circulation (Cheng et al., 1996), and then montelukast and its metabolites excreted via the bile (Balani et al., 1997). Analysis of human bile collected for 4–6 hours after montelukast oral intake indicate that montelukast undergoes extensive metabolism (Balani et al., 1997). The metabolites identified in human plasma and bile include montelukast acyl-β-D-glucuronide (M1), montelukast sulfoxide (M2), 25-hydroxy montelukast (M3), montelukast dicarboxylic acid (M4), 21(*R*)-hydroxy montelukast (M5a), 21(*S*)-hydroxy montelukast (M5b), and 36-hydroxy montelukast or 1,2 diol montelukast (M6) (Fig. 1) (Balani et al., 1997). Some of these metabolites show pharmacological activity, but their abundance in plasma is very low and thus it is improbable that they contribute to the effects of montelukast (Balani et al., 1997).

Montelukast 36-hydroxylation and then to M4 has been suggested as the main clearance mechanism of montelukast (Balani et al., 1997). However, owing to the lack of quantitative mass-balance study, the contribution of this or any other pathway to the overall montelukast elimination remains unclear. In addition, the specific enzymes responsible for montelukast clearance are inconsistent. In an earlier in vitro study and on the product label CYP2C9 and CYP3A4 are reported as the principal P450s in montelukast metabolism; CYP2C9 was considered selective toward montelukast 36-hydroxylation (Chiba et al., 1997). In contrast, recent in vitro studies implicate CYP2C8 in montelukast 36-hydroxylation (Filppula et al., 2011; VandenBrink et al., 2011), although close examination of the in vitro studies indicate that P450s other than CYP2C8 may also be involved. The potential role of CYP2C8 is further supported by the ability of montelukast to tightly bind to the CYP2C8 active site (Schoch et al., 2008) and to potently and competitively inhibit this enzyme in vitro (Walsky et al., 2005). In healthy volunteers, a markedly increased montelukast exposure along with diminished sequential metabolism via the 36-hydroxylation pathway was noted when montelukast was coadministered with gemfibrozil (Karonen et al., 2010, 2012). Gemfibrozil glucuronide is a potent mechanism-based inactivator of CYP2C8 (Shitara et al., 2004; Ogilvie et al., 2006; Backman et al., 2009). On the basis of the extent of

This work was supported by the National Institutes of Health National Institute of General Medical Sciences Grant [R01GM078501]. J.O.C. received financial support from the Brazilian National Council for Scientific and Technological Development (CNPq) and the Coordination for the Improvement of Higher Education Personnel (CAPES), Brazil.

dx.doi.org/10.1124/dmd.115.065763.

ABBREVIATIONS: ESI, electrospray ionization; HLM, human liver microsome; LC, liquid chromatography; MS/MS, tandem mass spectrometry; MTBE, methyl tertiary butyl ether; P450, cytochrome P450; thioTEPA, *N,N′,N″*-triethylenethiophosphoramide; UDPGA, uridine 5′-diphosphate glucuronic acid; UGT, uridine 5′-diphospho-glucuronosyltransferase.

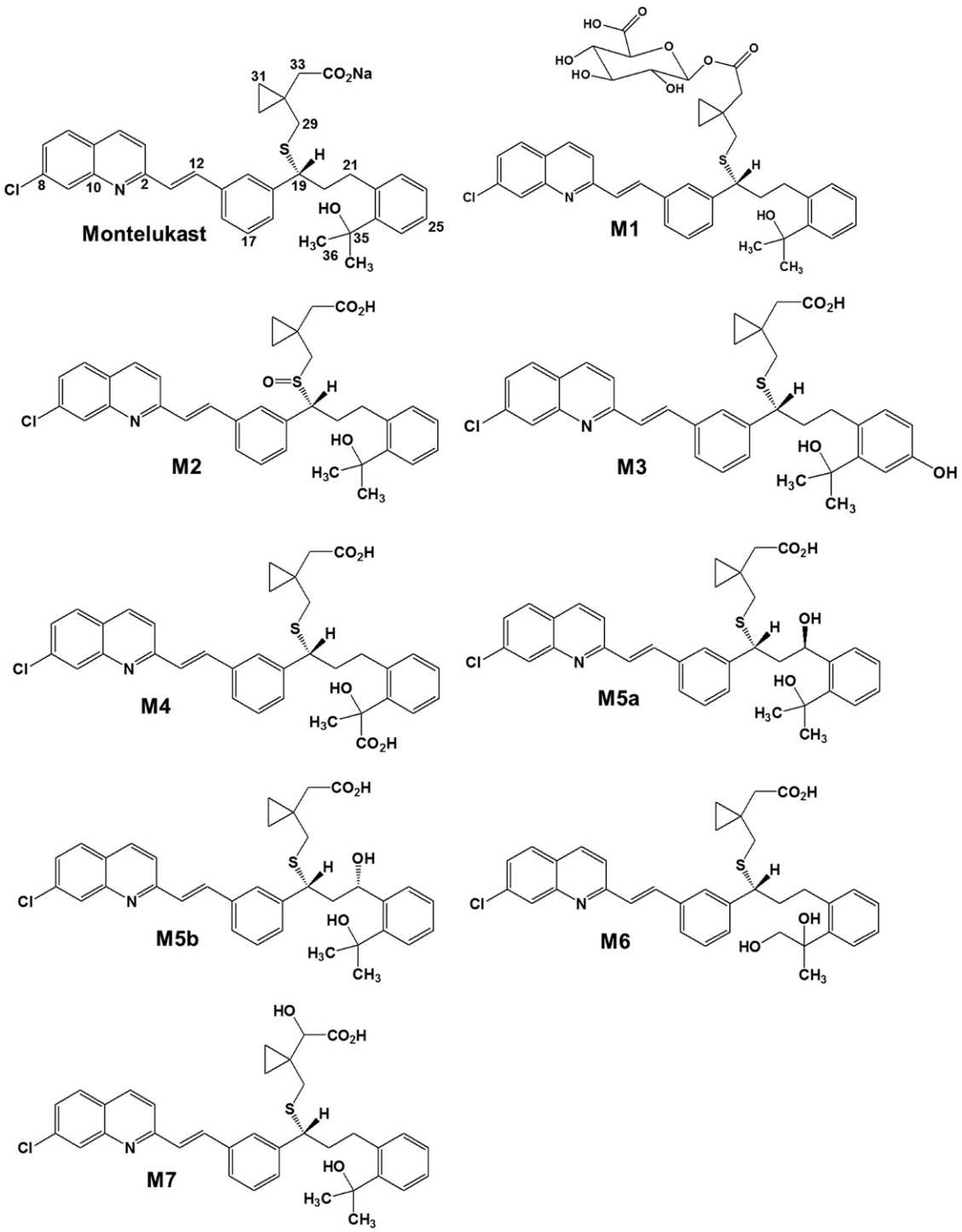

Fig. 1. Chemical structure of montelukast and its metabolites. M1, montelukast acyl-β-D-glucuronide; M2, montelukast sulfoxide; M3, 25-hydroxy montelukast; M4, montelukast dicarboxylic acid; M5a, 21(*R*)-hydroxy montelukast; M5b, 21(*S*)-hydroxy montelukast; M6, 36-hydroxy montelukast or 1,2 diol montelukast; M7, alpha-hydroxy-montelukast.

gemfibrozil-montelukast interaction, Karonen et al. (2012) suggested that CYP2C8 accounts for ~80% of the total montelukast clearance. As a result, montelukast was recommended as a sensitive probe of CYP2C8 activity in vivo (Karonen et al., 2010, 2012). However, the possibility that this interaction may involve effects of gemfibrozil on other drug disposition proteins in addition to inhibition of CYP2C8 cannot be ruled out. The potential for the presence of alternative mechanisms in montelukast disposition is supported by patterns of drug-drug interactions with montelukast. For example, the mechanism-based inactivator of CYP3A4, clarithromycin, increased montelukast $AUC_{0-\infty}$ by approximately 144% (Hegazy et al., 2012), whereas itraconazole (a potent CYP3A inhibitor) did not affect its disposition (Karonen et al., 2012). Clarithromycin is not known to inhibit CYP2C8.

The presence of carboxyl and hydroxyl sites in montelukast chemical structure (Fig. 1) indicate that montelukast may undergo direct conjugation

by uridine 5′-diphospho-glucuronosyltransferase (UGT) and/or sulfotransferases (SULT). Indeed, montelukast acyl-β-D-glucuronide has been identified in bile after the administration of montelukast to humans (Balani et al., 1997) and in vitro in human liver microsomes (Chiba et al., 1997), supporting UGT-mediated conjugation at the carboxylic site (Fig. 1). Similarly, montelukast may undergo direct conjugation at the hydroxyl site (Fig. 1), but no conjugated metabolite at this site has been identified in vitro or in vivo. Furthermore, the specific UGTs responsible for montelukast glucuronidation and the relative contribution of glucuronidation pathway to the overall montelukast metabolism remain unknown.

The purposes of this in vitro work were to use human liver microsomes (HLMs) and expressed P450s and UGTs to: 1) re-evaluate in detail the specific P450s involved in montelukast oxidation and 2) identify direct glucuronidation pathways of montelukast and the specific UGTs involved.

Materials and Methods

Chemicals

Montelukast sodium salt, montelukast 1,2 diol, montelukast sulfoxide, 21(*S*)-hydroxy montelukast, 21(*R*)-hydroxy montelukast, α-hydroxy montelukast, gemfibrozil 1-O-β-glucuronide, and montelukast acyl-β-D-glucuronide acetic acid salt were purchased from Toronto Research Chemicals (North York, Ontario, Canada). Uridine 5′-diphosphate glucuronic acid (UDPGA) trisodium salt, alamethicin, saccharic acid lactone, β-nicotinamide adenine dinucleotide phosphate (NADP) sodium salt, glucose-6-phosphate (G-6-P), G-6-P dehydrogenase from baker's yeast (*Saccharomyces cerevisiae*), pilocarpine hydrochloride, quercetin, quinidine, ketoconazole, sulfaphenazole, *N,N′,N″*-triethylenethiophosphoramide (thioTEPA), ticlopidine hydrochloride, troleandomycin triacetate, and gemfibrozil were purchased from Sigma-Aldrich (St. Louis, MO). The salts monobasic and dibasic sodium phosphate, tris(hydroxymethyl)aminomethane (tris base), sodium carbonate, magnesium chloride, and the solvents acetonitrile, methanol, methyl tertiary butyl ether (MTBE), formic acid, and hydrochloride acid were purchased from Fisher Scientific (Pittsburgh, PA).

Microsomal Preparations

Nine human liver microsomes (HLMs) from single donors, five pooled HLMs (n = 20–50), expressed human P450s (supersomes) (CYP1A2, CYP2A6, CYP2B6, CYP2C8, CYP2C9, CYP2C19, CYP2D6, CYP2E1, CYP3A4, CYP3A5, CYP4A11) with oxidoreductase and without coexpression of cytochrome b5 (expect CYP2E1), and expressed UGTs (UGT1A1, UGT1A3, UGT1A4, UGT1A6, UGT1A7, UGT1A8, UGT1A9, UGT1A10, UGT2B4, UGT2B7, UGT2B10, UGT2B15, UGT2B17) were purchased from BD Gentest (Woburn, MA) or Corning (Corning, NY). All microsomal preparations were stored at –80°C until analysis.

Liquid Chromatography–Tandem Mass Spectrometry Conditions to Analyze Montelukast and Its Oxidative and Glucuronide Metabolites

Montelukast and its metabolites were measured using a liquid chromatography–tandem mass spectrometry (LC-MS/MS) system. A triple quadrupole mass spectrometer API 2000 (Applied Biosystems, Foster City, CA) coupled with Shimadzu liquid chromatography system (Columbia, MD) consisting of a LC-20AB pump and SIL-20A HT autosampler was used. The chromatographic separation was achieved on a Luna C18 column (100 × 2.0 mm i.d.; 3 μm particle size; Phenomenex, Torrance, CA) at room temperature. Isocratic elution mode was applied using a mobile phase consisting of acetonitrile and water containing 0.1% formic acid in the proportion of 85/15 (v/v) for separation of montelukast and its oxidative metabolites and 82/18 (v/v) for separation of montelukast and montelukast glucuronides (injection volume, 10 μl; and flow rate, 0.2 ml/min). For the MS analysis, an electrospray ionization interface was selected and used in the positive ion mode. The MS parameters were initially optimized by infusion onto the MS/MS system of individual standard solutions of montelukast, montelukast acyl-β-D-glucuronide (M1), montelukast sulfoxide (M2), 21(R)-hydroxy montelukast (M5a), 21(*S*)-hydroxy montelukast (M5b), montelukast 1,2 diol (M6), and α-hydroxy-montelukast (M7) diluted in methanol/water (50:50), using a syringe pump at a flow rate of 10 μl/min. Authentic standards of 25-hydroxy montelukast (M3) and M-glucuronide (a new glucuronide metabolite) were not available to us and the transitions were monitored on the basis of the report of Balani et al. (1997) for 25-hydroxy or on the basis of values of montelukast acyl-glucuronide for M-glucuronide. The triple quadrupole was operated under the following conditions: curtain gas 25 psi, temperature 550°C, ion source gas 1 (GS1) 20 psi, ion source gas 2 (GS2) 55 psi, IonSpray Voltage (IS) 5500 V, and collision gas (CAD) 4 psi. For data acquisition, the triple quadrupole was operated in the selected reaction-monitoring mode (SRM). The ion transitions of the precursor ions to selected product ions monitored were m/z 586.2 to m/z 422.3 for montelukast, m/z 762 to m/z 422 for acyl-glucuronide and M-glucuronide, m/z 602 to m/z 422 for M2, m/z 602 to m/z 438 and m/z 602 to m/z 147 for M3 (Balani et al., 1997), m/z 602 to m/z 147 for M5a/b, m/z 602 to m/z 438 for M6, m/z 603 to m/z 422 for M7, and m/z 267 to m/z 226 for the internal standard (nevirapine). Data acquisition and processing were performed using the software Analyst version 1.5.1 (AB SCIEX, Ontario, Canada).

Stock solutions of montelukast, montelukast sulfoxide, montelukast 1,2 diol, 21(*S*)-hydroxy montelukast, 21(*R*)-hydroxy montelukast, and montelukast acyl-β-D-glucuronide were prepared at a concentration of 1.0 mg/ml in methanol and diluted to concentrations of 0.001–0.25 μM (montelukast and oxidative metabolites) or to 0.01–1.0 μM (montelukast acyl-β-D-glucuronide), which were then used to construct the calibration curves. Montelukast and its metabolites were quantified by using the ratio of peak area of the metabolite to peak area of internal standard. The concentrations of 25-hydroxy montelukast in the microsomal incubations were estimated by standard curves generated using montelukast, and the concentrations of M-glucuronide were estimated by standard curves generated using montelukast acyl-β-D-glucuronide. Detection showed a linear response ($r^2 > 0.99$) for montelukast and all its metabolites in the concentration range evaluated.

In Vitro Oxidative Metabolism of Montelukast

Incubation Conditions. Unless otherwise indicated, montelukast was dissolved and serially diluted in methanol to the required concentration. Any methanol was removed by drying in a speed vacuum before the addition of incubation components. To ensure solubilization of montelukast after drying, the following pilot experiments were performed. Montelukast was dried out and reconstituted with buffer and an aliquot of this solution was diluted in mobile phase prior to injection onto the LC-MS system. The chromatographic area of that solution was compared with the area of montelukast prepared in solution at the same final concentration and directly injected onto the LC-MS system (100%). The difference between the chromatographic areas was not significant, which indicates that the solubilization of montelukast was efficient in the procedure used for the incubation assays. Additionally, pilot incubations were performed initially where montelukast was incubated after drying and without drying (in solution). The chromatographic peak area of montelukast and its metabolites was not different between the incubations of the dried versus nondried samples. Since montelukast and its metabolites are sensitive to light, all incubation assays were performed in the absence of light. Pilot incubation experiments were performed using HLMs to identify potential metabolites of montelukast and optimize the conditions for incubation and LC-MS/MS analysis.

The incubation mixture (final volume, 250 μl) containing montelukast, 25 μl of HLMs (final concentration 0.25 mg protein/ml), and 125 μl of 0.2 M sodium phosphate buffer (pH 7.4) were preincubated for 5 minutes at 37°C. The reaction was initiated by adding 100 μl of a NADPH-generating system containing NADP (1.3 mM), glucose 6-phosphate (3.3 mM), $MgCl_2$ (3.3 mM), and glucose 6-phosphate dehydrogenase solution (0.4 IU/μl). The reaction was terminated at the specified time by the addition of 500 μl of ice-cold acetonitrile. Nevirapine (25 μl of 500 ng/ml in methanol) was added as an internal standard to the incubation sample, vortex-mixed, and centrifuged at 14,000 rpm for 5 minutes. The supernatant (600 μl) was transferred to a clean culture tube and extracted with 500 μl of saturated solution of sodium carbonate (Na_2CO_3) and 5 ml of MTBE. The mixture was vortex-mixed for 30 seconds and centrifuged at 36,000 rpm for 5 minutes as described elsewhere (Bharathi et al., 2009). The organic layer was removed and evaporated to dryness in a speed vacuum. The residue was reconstituted with 80 μl of mobile phase [acetonitrile/water + 0.1% formic

acid (85/15, v/v)] and an aliquot of 10 μl was injected onto the LC-MS/MS system. Negative control incubations including no substrate (montelukast), no NADPH-generating system, and no HLMs were carried out in parallel.

Using the incubation and LC-MS/MS assay conditions described above, linear conditions with respect to microsomal protein concentrations and duration of incubation for the formation of montelukast metabolites were defined. Thus, montelukast (1 μM) was incubated in HLMs (0.0–1.0 mg protein/ml) in the presence of the NADPH-generating system at 37°C across a range of incubation times (0–90 minutes). The 30 minute duration of incubation and 0.25 mg/ml microsomal protein concentration represented the linear conditions and were implemented subsequently unless stated.

Kinetic Analyses of Montelukast Oxidative Metabolism in HLMs. To determine the kinetics for the formation of montelukast oxidative metabolites, different concentrations of montelukast (0.05–15 μM) were incubated in duplicate with HLMs (0.25 mg protein/ml, $n = 2$), NADPH-generating system, and reaction buffer (0.2 M sodium phosphate buffer, pH 7.4) for 30 minutes at 37°C. The reaction was terminated and processed as described in the incubation condition above.

Correlation Analysis in HLMs. To determine correlations between the activity of individual P450 and formation rates of montelukast metabolites, montelukast was incubated in a panel of 14 characterized HLMs (9 single donors and five pooled HLMs). The total P450 contents, oxidoreductase, and activity of each P450 isoform determined by reaction phenotypes were as supplied (BD Gentest). Isoform-selective reactions phenotypes used were: phenacetin O-deethylase (CYP1A2), coumarin 7-hydroxylase (CYP2A6), (*S*)-mephenytoin N-demethylase (CYP2B6), paclitaxel 6α-hydroxylase (CYP2C8), diclofenac 4′-hydroxylase (CYP2C9), (*S*)-mephenytoin 4′-hydroxylase (CYP2C19), bufuralol 1′-hydroxylase (CYP2D6), chlorzoxazone 6-hydroxylase (CYP2E1), testosterone 6β-hydroxylase (CYP3A4), and lauric acid 12-hydroxylase (CYP4A11). Montelukast (1 μM) was incubated in triplicate with each HLM (final concentration 0.25 mg protein/ml), 0.2 M sodium phosphate buffer (pH 7.4), and NADPH-generating system for 30 minutes at 37°C. The reaction was terminated and processed as described above.

Metabolism of Montelukast by Expressed Human P450s. The metabolism of montelukast was measured in a panel of ten expressed human P450s (CYP1A2, 2A6, 2B6, 2C8, 2C9, 2C19, 2D6, 2E1, 3A4, and 3A5) to further characterize the specific isoforms involved. Montelukast (1 and 0.02 μM) was incubated with expressed human P450s (20 pmol) using the same conditions described above for incubation with HLMs. For the expressed P450s showing activity toward the montelukast metabolism and/or showing correlation in HLMs with metabolite formation (CYP2C8, CYP2C9, CYP2C19, CYP3A4, and CYP4A11), full kinetic studies were conducted by incubating a range montelukast concentrations (0.05–15 μM) in duplicate with expressed P450s (20 pmol), 0.2 M sodium phosphate buffer (pH 7.4), and a NADPH-generating system for 30 minutes at 37°C. The reaction was terminated and processed as described above for HLMs assays.

Chemical Inhibition of Montelukast Oxidative Metabolism. To determine the contribution of the P450s in the montelukast metabolism, the effect of chemical inhibitors on the formation rates of montelukast metabolites in HLMs were evaluated in the absence (control) and presence of the isoform-selective P450 inhibitor. Montelukast was incubated with the following known isoform-specific inhibitors: pilocarpine (50 μM) for CYP2A6, thioTEPA (50 μM) for CYP2B6, quercetin (150 μM) for CYP2C8, sulfaphenazole (25 μM) for CYP2C9, ticlopidine (5 μM) for CYP2C19, quinidine (50 μM) for CYP2D6, and troleandomycin (50 μM) and ketoconazole (1 μM) for CYP3A. The inhibitors were dissolved and diluted in methanol to required concentrations, with the exception of ticlopidine and thioTEPA, which were dissolved and diluted with water. All the solutions were stored at –80°C, with the exception of the solutions in water that were prepared fresh. Montelukast (1 and 0.02 μM) and the specific inhibitor in methanol were evaporated to dryness in speed vacuum before the addition of the incubation components. The inhibitors diluted in water were added in the incubation mixed without drying, and the volume (25 μl) was compensated by a decrease in the buffer volume (100 μl).

Competitive inhibitors (pilocarpine, thioTEPA, quercetin, sulfaphenazole, ticlopidine, quinidine, and ketoconazole) were preincubated for 5 minutes at 37°C with montelukast (1 and 0.02 μM), HLMs (25 μl, final concentration 0.25 mg/ml), and the 0.2 M sodium phosphate buffer pH 7.4 (125 μl). The reaction was initiated by addition of the NADPH-generating system (100 μl). After 30 minutes, the reaction was terminated by addition of 500 μl of ice-cold acetonitrile and submitted to liquid-liquid extraction as described above. The mechanism-based inhibitor, troleandomycin, was preincubated for 15 minutes at 37°C with 25 μl of HLMs (0.25 mg/ml), 0.2 M sodium phosphate buffer pH 7.4, (125 μl) and the NADPH-generating system (100 μl). After the preincubation, the total volume (250 μl) was transferred to a new tube containing montelukast (1 μM), and dried to start the montelukast metabolism. The reaction was performed at 37°C for 30 minutes and terminated by addition of 500 μl of ice-cold acetonitrile, following of a liquid-liquid extraction as described above.

In Vitro Direct Glucuronidation of Montelukast

Incubation Conditions. To determine montelukast glucuronidation, the HLMs were diluted in 0.1 M Tris-HCl buffer containing 5 mM $MgCl_2$ (pH 7.4) and activated by addition of alamethicin [dissolved in methanol/water, 50:50 (v/v)] at a final concentration of 50 μg/mg protein and left on ice for 15 minutes and gently agitated each 5 minutes. From pilot experiments, alamethicin concentration of 50 μg/mg protein represents the optimal concentration for HLMs activation. Activated HLMs (0.25 mg protein/ml) was preincubated with montelukast (1 μM) and 125 μl 0.1 M Tris-HCl buffer containing 5 mM $MgCl_2$ (pH 7.4) for 5 minutes at 37°C according to conditions described elsewhere (Walsky et al., 2012). The reaction was initiated by adding 100 μl of 5 mM UDPGA (total incubation volume, 250 μl). The reaction was terminated at the respective time points by addition of 100 μl of ice-cold acetonitrile. Nevirapine (25 μl of 500 ng/ml in methanol) was added as an internal standard to the incubation sample, vortex-mixed, and centrifuged at 14,000 rpm for 5 minutes. Supernatant (300 μl) was transferred to a clean culture tube and extracted with 500 μl of HCl (0.1 M) and 4 ml of MTBE. The mixture was vortex-mixed for 30 seconds and centrifuged at 36,000 rpm for 5 minutes. The organic layer was removed and evaporated to dryness. The residue was reconstituted with 80 μl of mobile phase [acetonitrile/water + 0.1% formic acid (82/18, v/v)] from which an aliquot of 10 μl was injected onto the LC-MS/MS system. Pilot incubation experiments were performed to identify potential montelukast glucuronides and optimize the conditions for incubation and LC-MS/MS analysis. Negative control incubations, including no substrate (montelukast), no UDPGA, and no HLMs, were carried out in parallel.

Using the incubation and LC-MS/MS UGT assay conditions described above, the linearity of montelukast glucuronide formation rate related to incubation time and protein concentration was established. Montelukast (1 μM) was incubated in activated HLMs (0.0–1.0 mg protein/ml) in the presence of UDPGA cofactor (5 mM) at 37°C across a range of incubation times (0–90 minutes). Formation rate of montelukast glucuronide were linear at 30 minutes duration of incubation and 0.25 mg/ml microsomal protein concentration.

Kinetic Analyses of Montelukast Glucuronidation. The kinetic studies of montelukast glucuronidation were performed in two different HLMs. Different concentrations of montelukast (0.05–25 μM) were incubated in duplicate with 0.1 M Tris-HCl buffer containing 5 mM of $MgCl_2$ (pH 7.4), activated HLMs (0.25 mg protein/ml), and UDPGA cofactor (5 mM) for 30 minutes at 37°C. The reactions were terminated and processed as described above for glucuronidation assay.

Metabolism of Montelukast by Expressed Human UGT Isoforms. To identify the specific UGTs involved, the glucuronidation of montelukast was tested in a panel of 13 expressed human UGTs. Montelukast (1 μM) was incubated in duplicate with each expressed UGT (UGT1A1, UGT1A3, UGT1A4, UGT1A6, UGT1A7, UGT1A8, UGT1A9, UGT1A10, UGT2B4, UGT2B7, UGT2B10, UGT2B15, UGT2B17) (final concentration 0.025 mg/ml protein), 0.1 M Tris-HCl buffer containing 5 mM of $MgCl_2$ (pH 7.4), and UDPGA cofactor (5 mM) for 30 minutes at 37°C. In contrast to HLMs, activation of expressed UGTs by alamethicin is not required (Walsky et al., 2012) and was not used in these experiments. As positive and negative controls, incubation with activated HLMs was run in parallel as described above for HLMs incubation conditions.

Among the expressed enzymes, UGT1A3 showed the highest activity toward montelukast glucuronidation. Therefore, full kinetics for the formation of montelukast glucuronides was determined by incubating montelukast (0.125–20 μM) with expressed UGT1A3 (0.025 mg/ml), 0.1 M Tris-HCl buffer containing 5 mM of $MgCl_2$ (pH 7.4), and UDPGA cofactor (5 mM) in duplicate for 30 minutes at 37°C. The reactions were terminated and processed as described above for glucuronidation assay.

Since clinical studies have shown that gemfibrozil markedly increases montelukast exposure, we also tested whether this interaction could be in part explained by inhibition of montelukast glucuronidation. Montelukast (1 μM) was incubated with HLMs (0.25 mg/ml protein) and cofactor in the absence and presence of an increasing concentration of gemfibrozil (0.5–250 μM) and its glucuronide metabolite, gemfibrozil 1-*O*-β-glucuronide (0.5–250 μM).

Data Analysis

Apparent kinetic parameters, maximum formation rate (V_{max}) and substrate concentration resulting in 50% of V_{max} (K_m), for montelukast oxidative and conjugated metabolites were estimated by fitting apparent formation rates of metabolites versus montelukast concentrations to a single-site Michaelis-Menten enzyme kinetic equation ($V = V_{max} \times [S]/(K_m + [S])$) using nonlinear regression analysis. In vitro intrinsic clearances (Cl_{int}) were given as V_{max}/K_m. Percent inhibition was calculated by comparing the inhibited activity with uninhibited activity (vehicle control). Correlation analyses were performed by nonparametric regression analysis using a Spearman's rank correlation test with GraphPad Prism software version 5 (GraphPad Software Inc., La Jolla, CA). $P < 0.05$ was regarded as statistically significant and all tests were two-sided. Data are presented as mean of duplicate and error bars show data variability for $N = 2$, unless stated otherwise.

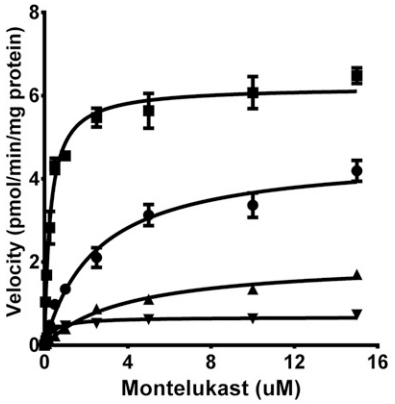

Fig. 2. Representative kinetic profiles of montelukast metabolism to 36 (1,2 diol)-(■), 21(*R*)- (●), 21(S)- (▲) and 25-hydroxy montelukast (▼) in HLMs. An increasing concentration of montelukast (0–15 μM) was incubated with HLMs (0.25 mg/ml) and a NADPH-generating system for 30 minutes at 37°C. Each point represents mean of duplicate incubations and error bars show data variability for $N = 2$.

Results

Montelukast Oxidative Metabolism. In the exploratory analyses of montelukast metabolism we could observe the formation of montelukast 1,2 diol, 21(*R*)-OH montelukast, 21(*S*)-OH montelukast, 25-OH montelukast, and montelukast sulfoxide. The sensitivity of the LC-MS/MS was too low to monitor the metabolite α-hydroxy montelukast. In agreement with a previous study (Filppula et al., 2011), the montelukast sulfoxide was present as contamination in the montelukast synthetic standard. Therefore, it was not possible to obtain an accurate quantification of montelukast sulfoxide produced during the metabolism of montelukast; consequently, it was not possible to identify precisely the P450s responsible for its formation. The formations of all other metabolites were dependent on the time of incubation, protein concentration, montelukast concentration, and NADPH-regeneration system. None of the montelukast metabolites were detected in the negative control incubations.

Kinetic Analysis of Montelukast Oxidative Metabolism in HLMs. Kinetic analyses for formation of montelukast oxidative metabolites were performed in two different HLMs preparations. Formation rates of montelukast metabolites were characterized by hyperbolic saturation curves and the kinetics were best described by the Michaelis-Menten equation. Representative kinetic profiles of montelukast metabolism to montelukast 1,2 diol, 21(*R*)-OH montelukast, 21(S)-OH montelukast, and 25-OH montelukast in HLMs are shown in Fig. 2. The corresponding kinetic parameters are summarized in Table 1. Based on the relative in vitro intrinsic clearance (Cl_{int}), montelukast 1,2 diol represents 83.5% of the total Cl_{int} of oxidative metabolism of montelukast, whereas the other metabolites tested together accounted for 16.5% of the total Cl_{int} [21(R)-OH-, 25-OH-, 21(S)-OH-montelukast accounting for 7.9%, 6.7%, and 1.9% of the total Cl_{int}, respectively]. Assuming that the contribution of other metabolites (sulfoxide and α-hydroxy-montelukast) to the overall oxidation of montelukast is small, montelukast 1,2 diol is the major oxidative metabolite of montelukast.

Correlation Analysis. The average ± S.D. formation rates (pmol/min per milligram of protein) of montelukast 1,2 diol, 21(*R*)-OH montelukast, 21(*S*)-OH montelukast, and 25-OH montelukast from montelukast oxidative metabolism in a panel of 14 HLMs were 7.86 ± 2.62 (range, 2.03–12.6; 6.2-fold), 1.48 ± 1.02 (range, 0.28–3.71; 13.4-fold), 0.46 ± 0.31 (range, 0.11–1.12; 10.6-fold), and 0.33 ± 0.12 (range, 0.09–0.51; 5.9-fold), respectively. Formation rates of montelukast metabolites in a panel of 14 characterized HLMs are depicted in the Supplemental Figure S1.

The correlation between the formation rates of montelukast 1,2 diol, 21 (R)-OH montelukast, 21(*S*)-OH montelukast, and 25-OH montelukast from montelukast oxidative metabolism and the activity of each P450 isoform in 14 HLMs are showed in Supplemental Table S1. Formation rate of 1,2 diol correlated significantly with the activity of CYP2C8, CYP2C19, CYP3A4, and CYP4A11; 21(*R*)-OH montelukast and 21 (*S*)-OH montelukast formation rates showed correlation with the activity of CYP2A6, CYP2B6, CYP2C19 and CYP3A4; and formation rates of 25-OH montelukast correlated significantly with the activity of CYP2A6, CYP2B6, CYP2C8, CYP2C19, CYP3A4, and CYP4A11. As shown in the Supplemental Table S1, all the metabolites show a good correlation with the activity of CYP2C19 ($r > 0.81$ and $p < 0.0004$) and CYP3A4 ($r > 0.68$ and $p < 0.007$). The correlation between the montelukast metabolites and the others enzymes, including total P450 contents (expect to 25-OH montelukast formation), was not significant ($r < 0.5$; $p > 0.05$).

The results from the correlation analysis showed involvement of multiple P450 enzymes in montelukast oxidation and these data did not provide very clear information about which enzyme may be mainly involved in the formation of montelukast oxidation. This is probably attributable to the use of a number pooled HLMs in these panels, which might have masked biologic intersubject variability in P450 activity.

TABLE 1

Kinetic parameters for the formation of montelukast 1,2 diol, 21(*R*)-OH montelukast, 21(S)-OH montelukast, and 25-OH montelukast from montelukast metabolism in two HLMs

The kinetic parameters for the formation of montelukast metabolites were estimated by fitting the velocity versus substrate concentration to a single-site Michaelis-Menten equation.

	HLM (HH837)			HLM (23418)		
Metabolites	V_{max}	K_m	CL_{int}	V_{max}	K_m	CL_{int}
Montelukast 1,2 diol	6.21	0.28	22.27	6.06	0.35	17.02
21(*R*)-OH montelukast	4.58	2.49	1.84	2.77	1.46	1.89
21(*S*)-OH montelukast	2.04	3.94	0.52	0.74	2.01	0.37
25-OH montelukast	0.67	0.40	1.68	0.41	0.27	0.37

V_{max}, pmol/min per milligram of protein; K_m, μM; CL_{int}, μl/min per milligram of protein.

Metabolism of Montelukast by Expressed Human P450s. Formation rates (pmol of metabolite/min per picomole of P450) of 1,2 diol, 21(*R*)-OH montelukast, 21(*S*)-OH montelukast, and 25-OH montelukast from montelukast (1 μM) in a panel of 10 expressed P450s are depicted in the Fig. 3. The isoforms that showed major contribution to the formation rates of montelukast oxidative metabolites were CYP2C8, CYP2C9, CYP3A4, and CYP3A5. CYP2C8 and CYP2C9 formed montelukast 1,2 diol at the highest rate; formation rate in CYP2C9 was 5.6-fold higher than in CYP2C8. CYP3A4 and CYP3A5 catalyzed montelukast 21(*R*)- and 21(*S*)-hydroxylation at the highest rate compared with other enzymes, but formation rates in CYP3A4 were higher than in CYP3A5 (8.1- and 5.9-fold, respectively). Multiple P450s (CYP2C8, CYP2C9, CYP2C19, and CYP3A4) were able to catalyze 25-hydroxylation of montelukast, but CYP2C8 and CYP2C9 catalyzed this reaction at the highest rate (4.4-fold higher in CYP2C9 than in CYP2C8). Despite the contamination of montelukast sulfoxide in the montelukast synthetic standard, CYP3A4 was identified as the main enzyme responsible for montelukast sulfoxide formation (Supplemental Fig. S2).

Formation rates (pmol of metabolite/min per picomole of P450) of montelukast oxidative metabolites were also evaluated from incubation 0.02 μM montelukast in a panel of 10 recombinant human P450s (Fig. 4). At this substrate concentration, only 1,2 diol and 21(*R*)-OH montelukast were quantifiable, whereas other metabolites were below limit of quantification. In agreement with the analysis using montelukast 1 μM, CYP2C8 and CYP2C9 formed 1,2 diol at the highest rate, with the formation rate in CYP2C9 1.8-fold higher than in CYP2C8. The formation of 21(*R*)-OH montelukast was catalyzed by CYP3A4, indicating its majority involvement in the formation of this metabolite.

Detailed kinetic analyses of montelukast were performed with selected P450s. The selection of P450s for kinetic analyses was made on the basis of the preliminary screening assay in the panel of P450s described above and on robust correlation observed in the HLMs panel. For example, CYP4A11, not described before as a P450 involved in the montelukast metabolism, showed significant correlation between its activity and the formation rates of montelukast 1,2 diol ($r = 0.81$ and $p = 0.0004$) and 25-OH montelukast ($r = 0.61$ and $p = 0.02$). Likewise, CYP2C19 showed significant correlation ($r > 0.81$ and $p < 0.0004$) with the formation rates of all four metabolites and was also included. Although the activities of CYP2A6 and CYP2B6 have shown significant correlation with formation rates of montelukast metabolites in HLMs, these P450s were not included in the kinetic analyses because they did not show relevant activity toward montelukast oxidation in the expressed P450s (Fig. 3).

Consistent with the results in HLMs, the kinetics for the formation of montelukast metabolites in expressed P450s was characterized by hyperbolic saturation curves and were best described by the Michaelis-Menten equation. The kinetic profiles of montelukast metabolism to montelukast 1,2 diol, 21(*R*)-OH montelukast, 21(*S*)-OH montelukast, and 25-OH montelukast in CYP2C8, CYP2C9, CYP2C19, CYP3A4, and CYP4A11 are shown in Fig. 5. The apparent kinetic parameters for the four metabolites are summarized in Table 2. The K_m values derived from expressed CYP2C8 and CYP2C9 for the formation of montelukast 1,2 diol were the lowest (K_m of 0.31 and 0.53 μM, respectively), which were close to that obtained from HLMs (average 0.32 μM) (Table 1), indicating that these same enzymes may be most significant in HLMs. The apparent in vitro intrinsic clearance (μl/min per picomole of P450) for the formation of montelukast 1,2 diol in CYP2C9 was 1.8-fold higher than CYP2C8. Together, these data suggest that these enzymes are comparably involved in the formation of montelukast 1,2 diol.

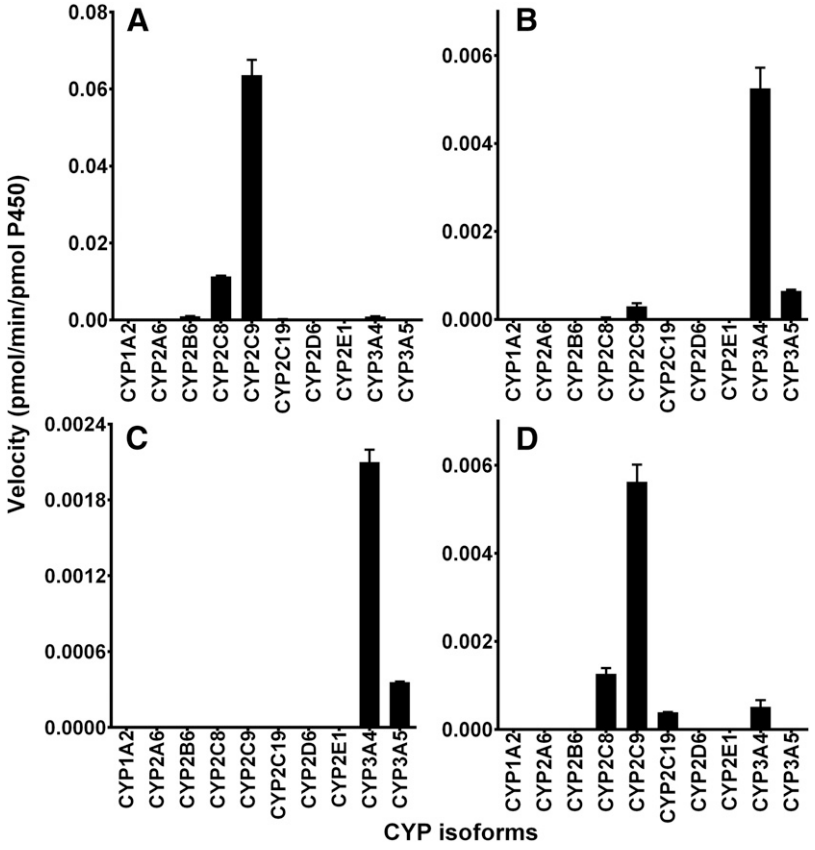

Fig. 3. Formation rates of montelukast metabolism to 36 (1,2 diol)- (**A**), 21(*R*)- (**B**), 21(*S*)- (**C**), and 25-hydroxy montelukast (**D**) in a panel of 10 expressed human P450 isoforms. Expressed P450 (20 pmol) was incubated with montelukast (1 μM) and NADPH-generating system (final volume, 250 μl) at 37°C for 30 minutes. The expressed human P450s used were coexpressed without cytochrome b5 with the exception of CYP2E1 which was expressed with cytochrome b5. Mean of duplicate incubations and error bars show in-data variability for $N = 2$ are presented.

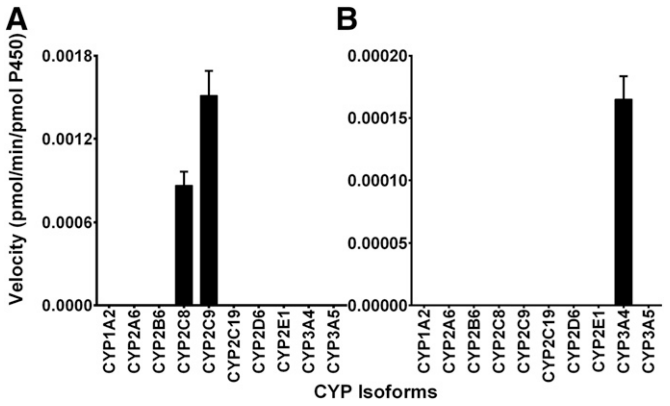

Fig. 4. Formation rates of montelukast metabolism to 36 (1,2 diol)- (A) and 21(*R*)-hydroxy montelukast (B) in a panel of 10 recombinant human P450s. Expressed P450 (20 pmol) was incubated with montelukast (0.02 μM) and NADPH-generating system (final volume, 250 μl) at 37°C for 30 minutes. The expressed human P450s used were coexpressed without cytochrome b5 with the exception of CYP2E1, which was expressed with cytochrome b5. 21(S)- and 25-hydroxymontelukast were below the limit of quantification at the substrate concentration tested. Mean of duplicate incubations and error bars showing data variability for $N = 2$ are presented.

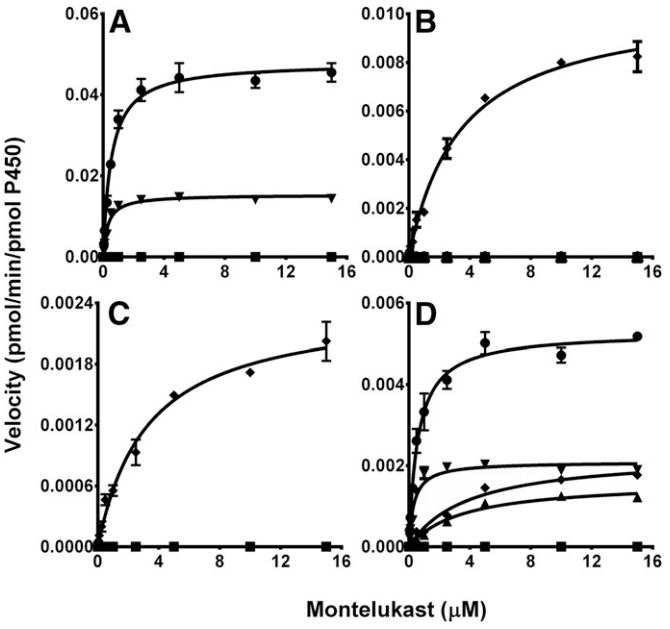

Fig. 5. Kinetics for the formation of 36 (1,2 diol)- (A), 21(*R*)- (B), 21(*S*)- (C) and 25-hydroxy montelukast (**D**) in expressed human CYP2C8 (▼), 2C9 (●), 2C19 (▲), 3A4 (♦), and 4A11 (■). A range of montelukast concentration (0–15 μM) was incubated with expressed P450 (20 pmol) and NADPH-generating system (final volume, 250 μl) at 37°C for 30 minutes. The expressed recombinant human P450s used were coexpressed without cytochrome b_5. The velocity (pmol/min per picomole of P450) versus montelukast concentration was fit to a single-site Michaelis-Menten equation. Each point represents mean of duplicate incubations and error bars show data variability for $N = 2$.

The kinetic analysis of 21(*R*)-OH montelukast and 21(*S*)-OH montelukast showed clearly that the CYP3A4, with the lowest K_m values (3.4 and 3.3 μM, respectively) and relatively higher apparent Cl_{int} of 0.0031 and 0.0007 μl/min per picomole of P450, respectively, is the main enzyme that catalyzes the formation of these metabolites. These metabolites showed a very similar K_m values but 21(*R*)-OH montelukast showed an apparent Cl_{int} 4.4-fold higher than 21(*S*)-OH montelukast, which suggest a higher capacity of CYP3A4 toward the formation of 21(R)-OH montelukast. The K_m values were close to that obtained from HLMs, ~2 and 3 μM, respectively, to 21(*R*)-OH montelukast and 21(S)-OH montelukast (Table 1).

The K_m values for the formation of 25-OH montelukast in CYP2C8, CYP2C9, CYP2C19 and CYP3A4 were 0.33, 0.59, 3.5, and 3.9 μM, and the in vitro Cl_{int} values were 0.006, 0.009, 0.0005, and 0.0006 μl/min per picomole of P450, respectively. Based on these kinetic analyses, CYP2C8 and CYP2C9 were the main enzymes involved in the 25-OH montelukast formation with a lesser contribution from CYP2C19 and CYP3A4.

Chemical Inhibition of Montelukast Metabolism. To further probe the contribution of each isoform, we tested the effect of P450-isoform–selective chemical inhibitors on montelukast oxidative metabolism in HLMs. As shown in Table 3, CYP3A inhibitors (ketoconazole and troleandomycin) markedly reduced (by >90%) the formation rates of 21(*R*)-OH montelukast and 21(*S*)-OH montelukast. These inhibitory effects in the formation rates of 21(*R*)-OH montelukast and 21(*S*)-OH montelukast are in agreement with the correlation analysis and the results from expressed P450s. Pilocarpine, thioTEPA, and sulfaphenazole, specific inhibitors of CYP2A6, CYP2B6, and CYP2C9, respectively, also inhibited the formation of these metabolites to a lesser extent (by ~40 and ~50%). The inhibitors quercetin (CYP2C8) and sulfaphenazole (CYP2C9) inhibited the formation rate of montelukast 1,2 diol by an average of ~52% and 43%, respectively. Ticlopidine, a dual inhibitor of CYP2B6 and CYP2C19, showed no relevant inhibitory effect (~8%) in the formation rate of montelukast 1,2 diol. The formation rate of 25-OH montelukast was inhibited mainly by quercetin, and sulfaphenazole, by an average of 27% and 22%, respectively. Moreover, inhibitory effects of others specific inhibitors were observed, but to a lower extent.

To further confirm the role of CYP2C8 and CYP2C9 in the formation of montelukast 1,2 diol, montelukast 1 and 0.02 μM was incubated with quercetin and sulfaphenazole, and with both inhibitors. The findings depicted at Fig. 6 confirm that CYP2C9 as well as CYP2C8 are the main enzymes involved in the formation of montelukast 1,2 diol at the concentrations of montelukast tested. The combination of quercetin and sulfaphenazole further reduced the formation of montelukast 1,2 diol by an average of 80.3 and 88.9% to montelukast 1 μM and 0.02 μM, respectively, compared with the ~52% and 43% inhibition observed when each inhibitor was tested individually.

Montelukast Glucuronidation. Upon incubation of montelukast with HLMs in the presence of UDPGA, two potential glucuronide metabolites denoted as M1 (major) and M-glucuronide (minor) (*m/z* 762.19) were observed at retention times of 3.3 minutes and 3.8 minutes, respectively (Fig. 7A). These peaks were not observed in negative control incubations. M1 glucuronide was consistent with montelukast acyl-β-D-glucuronide because its retention time and MS/MS fragmentation pattern was exactly the same as that of the synthetic standard montelukast acyl-β-D-glucuronide. M-glucuronide had the same molecular mass and fragmentation pattern as M1 and was monitored at the transition *m/z* 762 to *m/z* 422 like M1 after chromatographic separation. Although further studies are needed to confirm the specific structural features of M-glucuronide, the fact that montelukast has an alcohol functional group make it probable that this glucuronide is formed through direct glucuronidation of the hydroxyl site to an ether glucuronide. The formation of montelukast glucuronides was dependent on the time of incubation, protein concentration, montelukast concentration and UDPGA (data not shown). The linear conditions for the formation rate of montelukast acyl-β-D-glucuronide and M-glucuronide with respect to time of incubation and microsomal protein concentration was set at 30 minutes and 0.25 mg/ml in HLMs (and 0.025 mg/ml in expressed UGTs), respectively.

TABLE 2

Kinetic parameters for the formation of 1,2 diol, 21(*R*)-OH montelukast, 21(*S*)-OH montelukast, and 25-OH montelukast from montelukast in expressed in CYP2C8, CYP2C9, and CYP3A4

The kinetic parameters for the formation of montelukast metabolites were estimated by fitting the velocity versus substrate concentration to a single-site Michaelis-Menten equation.

	CYP2C8			CYP2C9			CYP3A4		
Metabolites	V_{max}	K_m	CL_{int}	V_{max}	K_m	CL_{int}	V_{max}	K_m	CL_{int}
Montelukast 1,2 diol	0.015	0.31	0.05	0.048	0.53	0.091	—	—	—
21(*R*)-OH montelukast	—	—	—	—	—	—	0.011	3.41	0.003
21(*S*)-OH montelukast	—	—	—	—	—	—	0.002	3.25	0.0007
25-OH montelukast	0.002	0.33	0.006	0.005	0.59	0.009	0.002	3.89	0.0006

V_{max}, pmol/min per picomole of protein; K_m, μM; Cl_{int}, μl/min per picomole of protein.

Kinetic Analysis of Montelukast Glucuronidation in HLMs. Kinetic analyses of montelukast glucuronidation were performed in two different HLM preparations. Formation rates of montelukast glucuronides were characterized by a hyperbolic saturation curves. The kinetic profiles of montelukast acyl-β-D-glucuronide and M-glucuronide in HLMs are depicted in Fig. 7B. In Table 4, the kinetic parameters for the formation of both glucuronides, derived using a single-site Michaelis-Menten equation, are summarized. On the basis of total in vitro intrinsic clearance (Cl_{int}) for glucuronidation, the in vitro Cl_{int} for the formation of acyl-β-D-glucuronide accounted for 88.2% and M-glucuronide for 11.8% of the total apparent Cl_{int} for glucuronidation (M1 + M-glucuronide), but since there was no synthetic standard for M-glucuronide (see *Materials and Methods*) the relative contribution of M-glucuronide to in vitro Cl_{int} presented here should be viewed tentative. If the in vitro Cl_{int} for montelukast oxidation (Table 1) is compared with Cl_{int} for montelukast glucuronidation (Table 4), Cl_{int} for total montelukast glucuronidation (to acyl-β-D-glucuronide + M-glucuronide) represented 84.8% of the total apparent in vitro Cl_{int} of montelukast (P450- and UGT-mediated Cl_{int}), whereas montelukast oxidative metabolism represented only 15.2% (Fig. 8). Glucuronidation was still predominant compared with oxidation (83.5% versus 16.5%), even when data on M-glucuronide was excluded.

Montelukast Glucuronidation by Expressed Human UGTs. Formation rates of montelukast acyl-β-D-glucuronide and M-glucuronide from 1 μM montelukast in a panel of 13 expressed UGTs are depicted in Fig. 7C. Of the isoforms tested, UGT1A3 catalyzed formation of both montelukast acyl-β-D-glucuronide and M-glucuronide. As with HLMs, formation rate of montelukast acyl-β-D-glucuronide by UGT1A3 was much higher than that of M-glucuronide.

Detailed kinetic analyses of montelukast glucuronidation were performed in UGT1A3 (Fig. 7D and Table 4). As with HLMs, the kinetics were characterized by a hyperbolic saturation curves and the data fit to a Michaelis-Menten equation. The apparent kinetic parameters for both glucuronides are summarized in Table 4. The K_m values derived from expressed UGT1A3 for the formation of montelukast acyl-β-D-glucuronide and M-glucuronide were ~2 μM and 0.37 μM, respectively, which were close to that obtained from HLMs (average 1.3 μM and 0.62 μM) (Table 4). The apparent in vitro Cl_{int} for the formation of montelukast acyl-β-D-glucuronide in UGT1A3 was 9.5-fold higher than M-glucuronide, indicating a higher capacity of UGT1A3 toward montelukast acyl-β-D-glucuronide formation.

Inhibition of Montelukast by Gemfibrozil and Its Glucuronide Metabolite in HLMs. In HLMs, gemfibrozil showed moderate inhibition of montelukast glucuronidation to acyl-β-D-glucuronide and M-glucuronide, with IC_{50} values of 83.4 μM and 37.6 μM, respectively (Supplemental Fig. 3). There was no meaningful effect of gemfibrozil 1-O-β-glucuronide on montelukast glucuronidation (<8% or at the highest concentration tested; data not shown).

Discussion

In recent years, montelukast has been recommended as a selective probe of CYP2C8 activity in vitro (Filppula et al., 2011; VandenBrink et al., 2011) and in vivo (Karonen et al., 2010, 2012) primarily on the basis of two assumptions: 36-hydroxylation to 1,2-diol and then to montelukast dicarboxylic acid (M4) is the main clearance mechanism of montelukast (Balani et al., 1997; Karonen et al., 2010, 2012); and this pathway is selectively catalyzed by CYP2C8 (Filppula et al., 2011; VandenBrink et al., 2011).

We found that 36-hydroxylation accounts for over 83% approximately of the total oxidative in vitro Cl_{int}, whereas 21- and 25-hydroxylation represent minor metabolic routes, which is consistent with previous in vitro (Chiba et al., 1997; Filppula et al., 2011; VandenBrink

TABLE 3

Inhibition of montelukast metabolism by P450 isoform–selective inhibitors in HLMs

Inhibition data in HLMs are mean ± S.D. (n = at least two independent experiments in duplicate). Rates of metabolite formation during incubation with the inhibitors are percentage of control (without inhibitor, at least four replicates) activity. Data are presented as mean ± S.D.

Inhibitor	P450 Inhibited	1,2 diol	21(*R*)-OH	21(*S*)-OH	25-OH
No inhibitor	Control	100.0	100.0	100.0	100.0
Pilocarpine	CYP2A6	83.2 ± 15.0	64.5 ± 12.6	60.9 ± 9.6	86.5 ± 9.7
ThioTEPA	CYP2B6	99.7 ± 10.4	56.0 ± 10.0	60.2 ± 9.7	96.9 ± 3.8
Quercetin	CYP2C8	48.4 ± 6.7	84.6 ± 7.7	96.7 ± 11.6	72.7 ± 5.2
Sulfaphenazole	CYP2C9	58.4 ± 5.8	52.1 ± 8.5	52.7 ± 4.5	78.0 ± 9.4
Ticlopidine	CYP2C19	92.0 ± 12.6	103.3 ± 4.0	107.2 ± 8.1	97.9 ± 13.2
Quinidine	CYP2D6	98.2 ± 13.4	87.5 ± 14.7	105.0 ± 5.5	101.4 ± 10.1
Troleandomycin	CYP3A	99.7 ± 7.4	7.9 ± 2.4	8.1 ± 2.8	80.0 ± 12.1
Ketoconazole	CYP3A	94.3 ± 7.8	5.6 ± 0.6	5.0 ± 0.8	97.5 ± 3.1

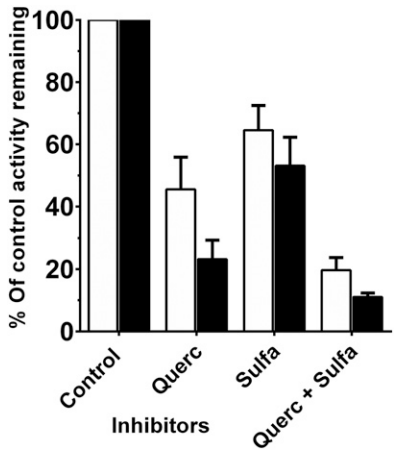

Fig. 6. Inhibition of formation rates of 36 (1,2 diol)-hydroxymontelukast from 1 μM (□) and 0.02 μM (■) montelukast by P450 isoform-selective chemical inhibitors in HLMs. Montelukast was incubated with HLMs (0.25 mg/ml), 0.2 M sodium phosphate buffer (pH 7.4) and NADPH-generating system (final volume, 250 μl) at 37°C for 30 minutes without and with selective inhibitors of CYP2C8 (quercetin, 10 μM), CYP2C9 (sulfaphenazole, 25 μM), and a combination of CYP2C8 and CYP2C9 (10 μM quercetin + 25 μM sulfaphenazole). Rates of metabolite formation during incubation with the inhibitors are presented as percentage of control (without inhibitor) activity. Mean of duplicate incubations and error bars showing data variability for $N = 2$ are presented. Sulfa, sulfaphenzole; Querc, quercetin.

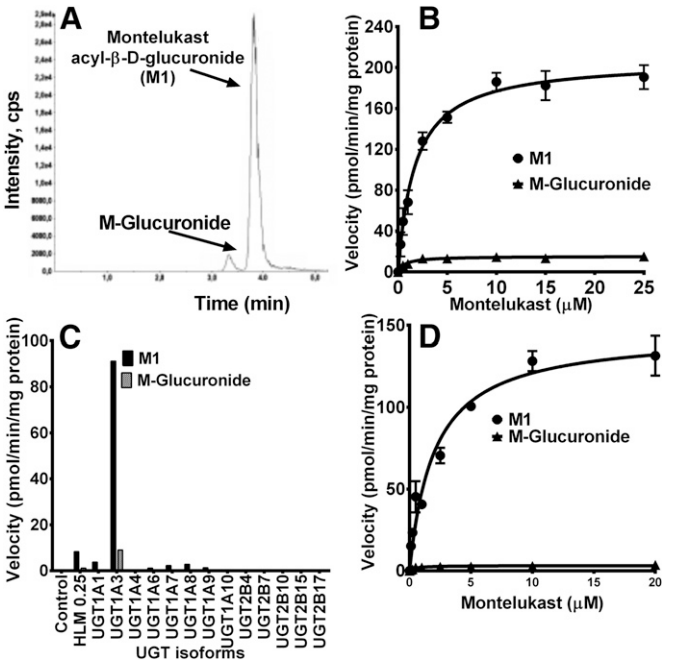

Fig. 7. Direct montelukast glucuronidation in HLMs and expressed UGTs. (A) LC-MS/MS representative chromatographic separation of montelukast and its glucuronides in incubation of montelukast (1 μM) with HLMs (0.25 mg/ml protein) and 5 mM UDPGA (see *Materials and Methods* for details). (B) Kinetic profiles of montelukast glucuronidation to montelukast acyl-β-D-glucuronide and M-glucuronide in HLM. An increasing concentration of montelukast (0–25 μM) was incubated with HLMs (0.25 mg/ml) and UDPGA (5 mM) for 30 minutes at 37°C. Each point represents average of duplicate incubations. (C) Formation rates of montelukast acyl-β-D-glucuronide and M-glucuronide from montelukast (1 μM) glucuronidation in a panel of 13 expressed UGTs. Montelukast (1 μM) was incubated with expressed UGT (0.025 mg/ml protein) and UDPGA (5 mM) (final volume, 250 μl) at 37°C for 30 minutes. (D) Kinetics for the formation of montelukast acyl-β-D-glucuronide and M-glucuronide in expressed UGT1A3. An increasing concentration of montelukast (0.125–20 μM) was incubated with expressed UGT1A3 (0.025 mg/ml protein) and 5 mM UDPGA (final volume, 250 μl) at 37°C for 30 minutes. The velocity (pmol/min per milligram of protein) versus montelukast concentration was fit to a single-site Michaelis-Menten equation. Mean of duplicate incubations and error bars showing data variability for $N = 2$ are presented.

et al., 2011) and in vivo (Balani et al., 1997) reports. Montelukast 1,2 diol undergoes further oxidation (carboxylation) to M4 in vitro (Fig. 9) (Filppula et al., 2011) and in vivo (Balani et al., 1997; Karonen et al., 2010). Since our experiments did not take sequential metabolism into account, we would expect that the actual in vitro CL_{int} for the formation of 1,2 diol to be higher than reported here. At therapeutically relevant montelukast concentrations, we show for the first time that both CYP2C8 and CYP2C9 contribute equally to the formation of 1,2 diol: 1) quercetin (CYP2C8) and sulphaphenazole (CYP2C9) inhibited montelukast 36-hydroxylation in HLMs (Fig. 6; Table 3); 2) coincubation of montelukast with quercetin and sulphaphenazole further reduced the formation of montelukast 1,2 diol (Fig. 6); 3) expressed CYP2C8 and CYP2C9 catalyzed the formation of 1,2 diol at the highest rate compared with other P450s (Table 2); 4) the K_m values for the formation of 1,2 diol derived from expressed CYP2C8 and CYP2C9 were close to each other (Table 2) and similar to those obtained in HLMs (Table 1), suggesting that CYP2C8 and CYP2C9 metabolize 1,2 diol formation with similar affinity. Consistent with previous reports (Chiba et al., 1997; Filppula et al., 2011; VandenBrink et al., 2011), we confirmed that the formation of 21(*R*)- and 21(*S*)-hydroxymontelukast and sulfoxide is mainly catalyzed by CYP3A4, whereas multiple P450s (CYP2C8 > 2C9 > 3A4 > 2C19) are involved in the 25-hydroxymontelukast formation. Our data in HLMs and expressed P450s reveal stereoselective montelukast 21-hydroxylation, mainly mediated by CYP3A4, as shown by V_{max} for the formation of 21(*R*)-OH- higher (and thus higher in vitro Cl_{int}) than that for 21(*S*)-OH-montelukast; there was no difference in enzyme-substrate affinity as the K_m values for the formation of the two enantiomers were similar.

Our data broadly concur with previous in vitro studies showing involvement of CYP2C9 or CYP2C8, but ours is the first to report approximately equal participation of both enzymes toward montelukast 36-hydroxylation. Chiba et al. (1997) reported that montelukast 36-hydroxylation is exclusively catalyzed by CYP2C9, but the role of other enzymes, including CYP2C8, might have been masked, as supratherapeutic substrate concentrations were used. The product label of montelukast states that CYP2C9 and CYP3A are important in its metabolism. Evidence implicating CYP2C8 in montelukast 36-hydroxylation to 1,2-diol and then to M4 has been accumulating in recent years. Montelukast has been shown to tightly bind to the CYP2C8 active site (Schoch et al., 2008) and to be a potent in vitro competitive inhibitor of CYP2C8 (K_i, below 10 nM) (Walsky et al., 2005). Recently, two independent laboratories have suggested that CYP2C8 may be the main enzyme responsible for 36-hydroxylation of montelukast (Filppula et al., 2011; VandenBrink et al., 2011), but close examination of these data does not fully exclude involvement of other P450s. One notable difference between the previous studies and the present study is the use recombinant P450s coexpressed with cytochrome b5 to generate depletion and/or kinetic parameters (Filppula et al., 2011; VandenBrink et al., 2011) and without coexpression of cytochrome b5 (current study). Considering the known effect of cytochrome b5 on catalytic efficiency and binding of many P450s, extrapolation of data obtained with cytochrome b5 coexpression to HLMs and in vivo may be limited. We believe that our in vitro data showing involvement of CYP2C8 and CYP2C9 are solid and supported by multiple approaches in HLMs and expressed P450s. Particularly, the additive inhibitory effect of sulfaphenazole and quercetin (Fig. 6) on 36-hydroxylation of montelukast (0.02 μM and 1 μM) in HLMs provides strong support to the significant involvement of CYP2C9 in montelukast 1,2 diol formation.

TABLE 4

Kinetic parameters for the formation of montelukast acyl-β-D-glucuronide and M-glucuronide from montelukast in two HLMs and expressed UGT1A3

The kinetic parameters for the formation of montelukast glucuronides were estimated by fitting the velocity versus substrate concentration to a single-site Michaelis-Menten equation.

	Acyl-β-D-Glucuronide			M-Glucuronide		
	V_{max}	K_m	CL_{int}	V_{max}	K_m	CL_{int}
HLM (HH837)	207.4	1.72	120.2	14.7	0.71	20.6
HLM (23418)	101.1	0.90	112.5	5.59	0.53	10.5
UGT 1A3	145.1	1.97	73.5	2.86	0.37	7.78

V_{max}, pmol/min per milligram of protein; K_m, μM; Cl_{int}, μl/min per milligram of protein.

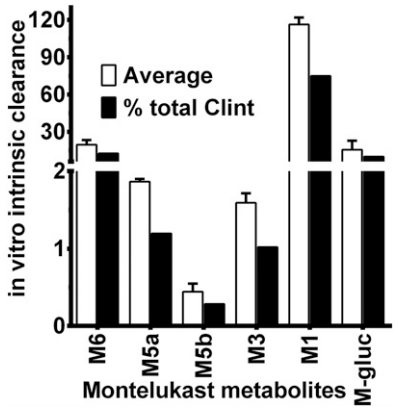

Fig. 8. Apparent in vitro intrinsic clearance (□) of montelukast 1,2 diol (M6), 21(*R*)-OH montelukast (M5a), 21(*S*)-OH montelukast (M5b), 25-OH montelukast (M3), montelukast acyl-β-D-glucuronide (M1) and M-glucuronide (M-gluc). Average: represents the average of duplicate incubations in two HLMs (Cl_{int}: μl/min per milligram of protein). % total Cl_{int} (■), contribution of each metabolite (%) in the total apparent Cl_{int} of montelukast (P450- and UGT-mediated). Mean of percentage of total Cl_{int} ($n = 2$ HLMs) and error bars showing data variability for $N = 2$ are presented.

An acyl-glucuronide of montelukast was detected in human bile collected after oral administration of montelukast as a minor metabolite (Balani et al., 1997) and in an in vitro microsomal study (Chiba et al., 1997). However, the role of glucuronidation in montelukast elimination and the specific enzymes involved has generally gained little attention. In the present study, we identified two glucuronide peaks (Fig. 7A). The major peak was confirmed to be montelukast acyl-β-D-glucuronide, on the basis of the same retention time and fragmentation pattern with synthetic montelukast acyl-β-D-glucuronide standard. The second minor peak has not been reported before (M-glucuronide). Intramolecular acyl migration is well described in the literature for many acyl glucuronides. Since we had no standard for M-glucuronide and because we did not performed the isomerization experiment, we could not completely rule out that this peak is not attributable to acyl migration. However, we speculate that this metabolite represents a new ether glucuronide of montelukast rather than acyl migration. First, there is a second hydroxyl group within montelukast molecule that may undergo glucuronidation. Second, although at physiologic pH (7.4) the acyl glucuronides are susceptible to hydrolysis and acyl migration, the short incubation time and immediate treatment of the samples in acid conditions employed here favor stability of acyl glucuronide, making acyl migration improbable. Third, other authors have reported that acyl glucuronide of montelukast is stable and does not undergo isomerization, probably owing to steric hindrance (Sawamura et al., 2010).

Upon kinetic analysis in HLMs, the K_m values derived for the two metabolites were similar (below 2 μM), although the V_{max} values and thus in vitro Cl_{int} was much higher for acyl-glucuronide than for M-glucuronide. This regioselective glucuronidation is probably attributable to steric hindrance at the hydroxyl group of montelukast. The K_m value for the formation of acyl-glucuronide reported here was over 9-fold lower than previously reported in HLMs (Chiba et al., 1997), but direct comparison may be difficult considering the marked difference in the assay conditions and in the substrate concentrations used for the saturation curves (0–25 μM in the present study versus 100–500 μM in their study). Subsequent experiments reveal for the first time that UGT1A3 is the main enzyme responsible for the formation of acyl- and M-glucuronides: In a panel of expressed UGTs, UGT1A3 catalyzed them at the highest rate; and the K_m value derived from expressed UGT1A3 was close to those derived from HLMs, suggesting involvement of the same enzyme in HLMs.

Comparison of the in vitro Cl_{int} for P450-mediated oxidation and UGT-mediated glucuronidation suggest higher contribution of direct glucuronidation (acyl-glucuronide + M-glucuronide) than total oxidation to the overall montelukast clearance (Fig. 8). Since the K_m values for oxidation and glucuronidation were comparable, substantially higher V_{max} and thus higher Cl_{int} values were noted for the formation of glucuronides compared to the values for the formation of oxidative metabolites. Our data broadly agree with a previous study showing much higher Cl_{int} for the formation of acyl-glucuronide than any of the oxidative metabolites in HLMs (Chiba et al. (1997), although their findings were not discussed in the context of the contribution of oxidation versus glucuronidation to montelukast metabolism. In contrast, relatively low yield of acyl-glucuronide was reported in human bile collected for a brief period of time (4-6 hours) (Balani et al., 1997), which could be attributable in part to low stability of acyl glucuronides, particularly at neutral or slightly alkaline conditions during sample preparation (Faed, 1984; Trontelj, 2012). Since UGT1A3 is expressed in the gut and liver (Ritter, 2007), it is also possible that montelukast is conjugated before it reaches the systemic circulation. A recent in vitro study using human primary hepatocytes suggested that a P450-mediated pathway may be quantitatively more important than a UGT-mediated pathway (Jinno et al., 2014), but nonselective inhibitors of P450s and UGTs were used at very high concentrations to dissect this contribution. In addition, the UGT inhibitor used in that study did not fully inhibited formation of acyl glucuronide (only by 35%).

Clinical studies have reported that gemfibrozil markedly increased exposure of montelukast and decreased exposure of 1,2-diol and its downstream metabolite (M4) (Karonen et al., 2012). Since gemfibrozil 1-O-β-glucuronide is a potent mechanism-based inhibitor of CYP2C8 (Shitara et al., 2004; Ogilvie et al., 2006; Backman et al., 2009), it is plausible to suggest that the mechanism of this interaction is inhibition of CYP2C8. The authors estimated CYP2C8 to account for ~80% of montelukast metabolism in humans (Karonen et al., 2010, 2012) and recommended montelukast as a selective CYP2C8 probe of activity in vivo. However, gemfibrozil inhibits multiple drug disposition proteins other than CYP2C8 to varying degree (Wen et al., 2001; Prueksaritanont et al., 2002; Shitara et al., 2004; Noe et al., 2007; Mougey et al., 2009; Gan et al., 2010), and it is possible the observed in vivo effect of gemfibrozil may have been mediated in part through inhibition of other pathways in addition to the known inhibition of CYP2C8. Consistent with a previous study showing inhibition of expressed UGT1A3 by gemfibrozil (Gan et al., 2010), our in vitro data show modest inhibition of montelukast glucuronidation in HLMs, although the potency of this inhibition appears too low to explain the effect of gemfibrozil on montelukast exposure in vivo. While gemfibrozil potently inhibits CYP2C9 in vitro (Wen et al., 2001), the

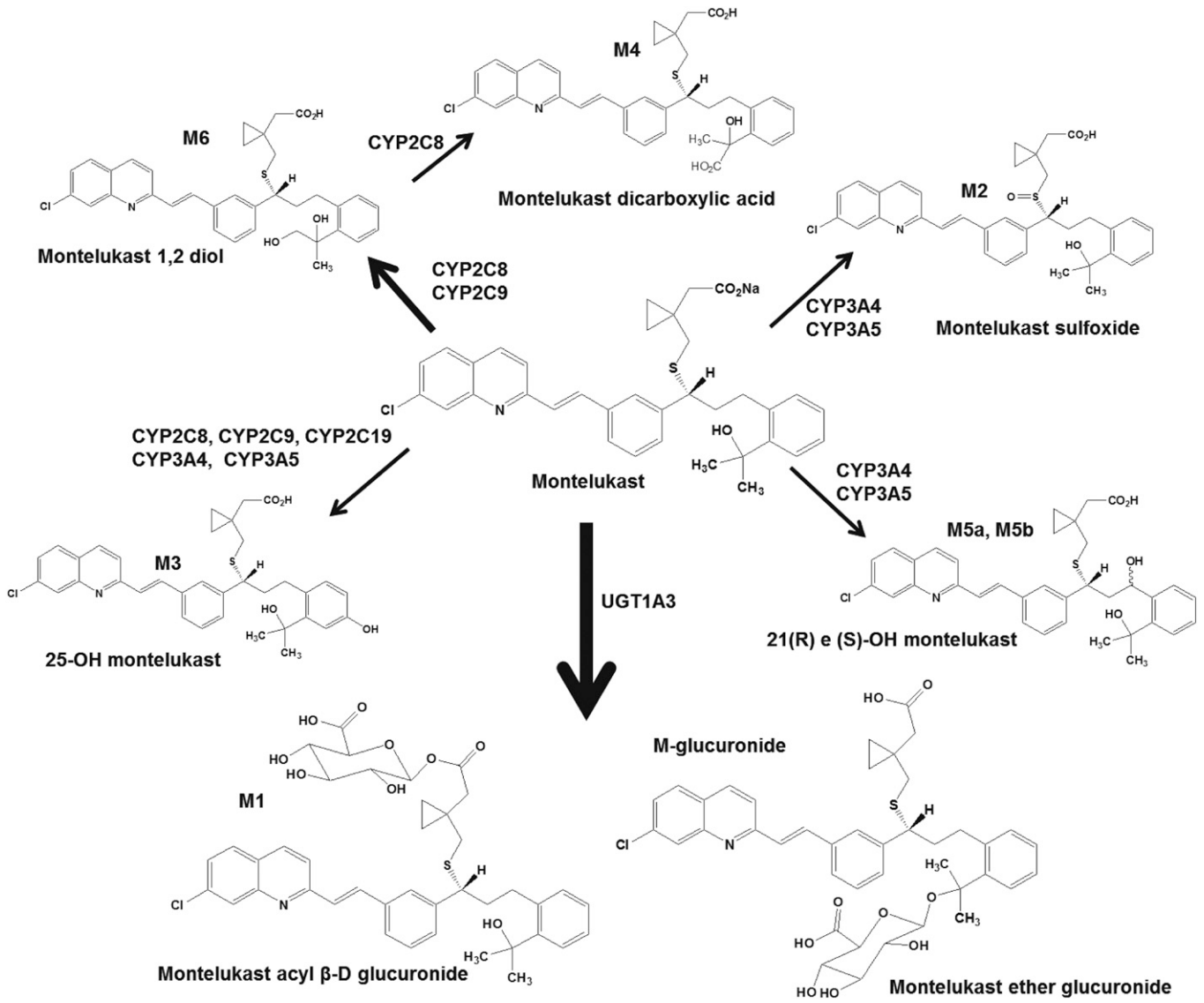

Fig. 9. Proposed human oxidation and glucuronidation metabolic pathways of montelukast and the specific enzymes involved [data summarized from the present study and published literature (Chiba et al., 1997; Karonen et al., 2010; Filppula et al., 2011)].

in vivo effect is modest (Niemi et al., 2001). The mechanism-based inactivator of CYP3A4 clarithromycin increases montelukast exposure by ~144%, whereas fluconazole decreased montelukast exposure by >30% (Hegazy et al., 2012). It is improbable that this effect is mediated via CYP3A or CYP2C8, because itraconazole, another strong CYP3A4 inhibitor, had no effect on the systemic exposure of montelukast (Karonen et al., 2012), and clarithromycin and fluconazole are not known to inhibit CYP2C8. These data suggest involvement of yet unidentified pathways of montelukast disposition, possibly drug transporters (Hegazy et al., 2012).

In summary, we present new insight into montelukast metabolism in vitro (Fig. 9). We provide the first in vitro evidence that CYP2C8 and CYP2C9 are equally important in 36-hydroxylation to 1,2-diol at therapeutically relevant concentrations. We identified a novel montelukast glucuronide that appears consistent with an ether glucuronide. In our hands, montelukast glucuronidation to acyl glucuronide and M-glucuronide by UGT1A3 appears to be the main clearance mechanism for montelukast in vitro. However, we recognize the apparent discrepancy between our in vitro data showing involvement of CYP2C9 and UGT1A3 in montelukast metabolism and the clinical pharmacokinetic interaction with gemfibrozil. Further studies designed to assess the clinical relevance of our in vitro findings and interplay between different disposition mechanisms appears warranted. To this end, we are conducting a clinical study designed to determine the effect of efavirenz on the metabolism and pharmacokinetics a single 10-mg montelukast in healthy volunteers (ClinicalTrials.gov Identifier: NCT02401256). The assumption that a gemfibrozil-montelukast interaction is mainly mediated by CYP2C8 may also need further validation using other approaches (e.g., use of other selective CYP2C8 inhibitors).

Authorship Contributions

Participated in research design: Cardoso, Desta.
Conducted experiments: Cardoso, Lu.
Contributed new reagents or analytic tools: Desta.
Performed data analysis: Cardoso, Desta, Oliveira.
Wrote or contributed to the writing of the manuscript: Cardoso, Desta, Oliveira.

References

Backman JT, Honkalammi J, Neuvonen M, Kurkinen KJ, Tornio A, Niemi M, and Neuvonen PJ (2009) CYP2C8 activity recovers within 96 hours after gemfibrozil dosing: estimation of CYP2C8 half-life using repaglinide as an in vivo probe. *Drug Metab Dispos* **37**:2359–2366.

Balani SK, Xu X, Pratha V, Koss MA, Amin RD, Dufresne C, Miller RR, Arison BH, Doss GA, and Chiba M, et al. (1997) Metabolic profiles of montelukast sodium (Singulair), a potent cysteinyl leukotriene1 receptor antagonist, in human plasma and bile. *Drug Metab Dispos* **25**:1282–1287.

Bharathi DV, Hotha KK, Jagadeesh B, Mullangi R, and Naidu A (2009) Quantification of montelukast, a selective cysteinyl leukotriene receptor (CysLT1) antagonist in human plasma by liquid chromatography-mass spectrometry: validation and its application to a human pharmacokinetic study. *Biomed Chromatogr* **23**:804–810.

Cheng H, Leff JA, Amin R, Gertz BJ, De Smet M, Noonan N, Rogers JD, Malbecq W, Meisner D, and Somers G (1996) Pharmacokinetics, bioavailability, and safety of montelukast sodium (MK-0476) in healthy males and females. *Pharm Res* **13**:445–448.

Chiba M, Xu X, Nishime JA, Balani SK, and Lin JH (1997) Hepatic microsomal metabolism of montelukast, a potent leukotriene D4 receptor antagonist, in humans. *Drug Metab Dispos* **25**: 1022–1031.

Dahlén SE, Hedqvist P, Hammarström S, and Samuelsson B (1980) Leukotrienes are potent constrictors of human bronchi. *Nature* **288**:484–486.

De Lepeleire I, Reiss TF, Rochette F, Botto A, Zhang J, Kundu S, and Decramer M (1997) Montelukast causes prolonged, potent leukotriene D4-receptor antagonism in the airways of patients with asthma. *Clin Pharmacol Ther* **61**:83–92.

Faed EM (1984) Properties of acyl glucuronides: implications for studies of the pharmacokinetics and metabolism of acidic drugs. *Drug Metab Rev* **15**:1213–1249.

Filppula AM, Laitila J, Neuvonen PJ, and Backman JT (2011) Reevaluation of the microsomal metabolism of montelukast: major contribution by CYP2C8 at clinically relevant concentrations. *Drug Metab Dispos* **39**:904–911.

Gan J, Chen W, Shen H, Gao L, Hong Y, Tian Y, Li W, Zhang Y, Tang Y, and Zhang H, et al. (2010) Repaglinide-gemfibrozil drug interaction: inhibition of repaglinide glucuronidation as a potential additional contributing mechanism. *Br J Clin Pharmacol* **70**:870–880.

Hegazy SK, Mabrouk MM, Elsisi AE, and Mansour NO (2012) Effect of clarithromycin and fluconazole on the pharmacokinetics of montelukast in human volunteers. *Eur J Clin Pharmacol* **68**:1275–1280.

Jinno N, Tagashira M, Tsurui K, and Yamada S (2014) Contribution of cytochrome P450 and UDT-glucuronosyltransferase to the metabolism of drugs containing carboxylic acid groups: risk assessment of acylglucuronides using human hepatocytes. *Xenobiotica* **44**:677–686.

Jones TR, Metters K, and Evans AJ (2001) Preclinical pharmacological studies with montelukast (Singulair), a selective cysteinyl leukotriene receptor(CysLT1) antagonist. *Clinical and Experimental Allergy Reviews* **1**:205–209.

Karonen T, Filppula A, Laitila J, Niemi M, Neuvonen PJ, and Backman JT (2010) Gemfibrozil markedly increases the plasma concentrations of montelukast: a previously unrecognized role for CYP2C8 in the metabolism of montelukast. *Clin Pharmacol Ther* **88**:223–230.

Karonen T, Neuvonen PJ, and Backman JT (2012) CYP2C8 but not CYP3A4 is important in the pharmacokinetics of montelukast. *Br J Clin Pharmacol* **73**:257–267.

Knorr B, Matz J, Bernstein JA, Nguyen H, Seidenberg BC, Reiss TF, and Becker A; Pediatric Montelukast Study Group (1998) Montelukast for chronic asthma in 6- to 14-year-old children: a randomized, double-blind trial. *JAMA* **279**:1181–1186.

Lewis RA, Austen KF, and Soberman RJ (1990) Leukotrienes and other products of the 5-lipoxygenase pathway. Biochemistry and relation to pathobiology in human diseases. *N Engl J Med* **323**:645–655.

Mougey EB, Feng H, Castro M, Irvin CG, and Lima JJ (2009) Absorption of montelukast is transporter mediated: a common variant of OATP2B1 is associated with reduced plasma concentrations and poor response. *Pharmacogenet Genomics* **19**:129–138.

Niemi M, Neuvonen PJ, and Kivistö KT (2001) Effect of gemfibrozil on the pharmacokinetics and pharmacodynamics of glimepiride. *Clin Pharmacol Ther* **70**:439–445.

Noé J, Portmann R, Brun M-E, and Funk C (2007) Substrate-dependent drug-drug interactions between gemfibrozil, fluvastatin and other organic anion-transporting peptide (OATP) substrates on OATP1B1, OATP2B1, and OATP1B3. *Drug Metab Dispos* **35**: 1308–1314.

Ogilvie BW, Zhang D, Li W, Rodrigues AD, Gipson AE, Holsapple J, Toren P, and Parkinson A (2006) Glucuronidation converts gemfibrozil to a potent, metabolism-dependent inhibitor of CYP2C8: implications for drug-drug interactions. *Drug Metab Dispos* **34**:191–197.

Prueksaritanont T, Zhao JJ, Ma B, Roadcap BA, Tang C, Qiu Y, Liu L, Lin JH, Pearson PG, and Baillie TA (2002) Mechanistic studies on metabolic interactions between gemfibrozil and statins. *J Pharmacol Exp Ther* **301**:1042–1051.

Reiss TF, Altman LC, Chervinsky P, Bewtra A, Stricker WE, Noonan GP, Kundu S, and Zhang J (1996) Effects of montelukast (MK-0476), a new potent cysteinyl leukotriene (LTD4) receptor antagonist, in patients with chronic asthma. *J Allergy Clin Immunol* **98**:528–534.

Ritter JK (2007) Intestinal UGTs as potential modifiers of pharmacokinetics and biological responses to drugs and xenobiotics. *Expert Opin Drug Metab Toxicol* **3**:93–107.

Sawamura R, Okudaira N, Watanabe K, Murai T, Kobayashi Y, Tachibana M, Ohnuki T, Masuda K, Honma H, and Kurihara A, et al. (2010) Predictability of idiosyncratic drug toxicity risk for carboxylic acid-containing drugs based on the chemical stability of acyl glucuronide. *Drug Metab Dispos* **38**:1857–1864.

Schoch GA, Yano JK, Sansen S, Dansette PM, Stout CD, and Johnson EF (2008) Determinants of cytochrome P450 2C8 substrate binding: structures of complexes with montelukast, troglitazone, felodipine, and 9-cis-retinoic acid. *J Biol Chem* **283**:17227–17237.

Shitara Y, Hirano M, Sato H, and Sugiyama Y (2004) Gemfibrozil and its glucuronide inhibit the organic anion transporting polypeptide 2 (OATP2/OATP1B1:SLC21A6)-mediated hepatic uptake and CYP2C8-mediated metabolism of cerivastatin: analysis of the mechanism of the clinically relevant drug-drug interaction between cerivastatin and gemfibrozil. *J Pharmacol Exp Ther* **311**:228–236.

Trontelj J (2012) Quantification of glucuronide metabolites in biological matrices by LC-MS/MS, in: *Tandem Mass Spectrometry—Applications and Principles* (Prasain JK ed), InTech ISBN 978-953-51-0141-3, available at: http://www.intechopen.com/books/tandem-mass-spectrometry-applications-and-principles/quantification-of-glucuronide-metabolites-in-biological-matrices-by-lc-ms-ms.

VandenBrink BM, Foti RS, Rock DA, Wienkers LC, and Wahlstrom JL (2011) Evaluation of CYP2C8 inhibition in vitro: utility of montelukast as a selective CYP2C8 probe substrate. *Drug Metab Dispos* **39**:1546–1554.

Walsky RL, Bauman JN, Bourcier K, Giddens G, Lapham K, Negahban A, Ryder TF, Obach RS, Hyland R, and Goosen TC (2012) Optimized assays for human UDP-glucuronosyltransferase (UGT) activities: altered alamethicin concentration and utility to screen for UGT inhibitors. *Drug Metab Dispos* **40**:1051–1065.

Walsky RL, Obach RS, Gaman EA, Gleeson JPR, and Proctor WR (2005) Selective inhibition of human cytochrome P450 2C8 by montelukast. *Drug Metab Dispos* **33**:413–418.

Wen X, Wang JS, Backman JT, Kivistö KT, and Neuvonen PJ (2001) Gemfibrozil is a potent inhibitor of human cytochrome P450 2C9. *Drug Metab Dispos* **29**:1359–1361.

Address correspondence to: Dr. Zeruesenay Desta, Department of Medicine, Division of Clinical Pharmacology, Indiana University School of Medicine, R2, Room 425, 950 West Walnut St., Indianapolis, IN 46202-5188. E-mail: zdesta@iupui.edu